THE NUMERICAL COMPARISON STUDY ON THE EFFECT OF THE ANTI-ICING METHODS ON THERMAL STRESS DISTRIBUTION OF NACELLE LIP-SKIN

By:

SITI ROSYADA BINTI MUHAMAD YUSLI

(Matrix no: 125046)

Supervisor:

Dr. Mohd Azmi bin Ismail

May 2018

This dissertation is submitted to

Universiti Sains Malaysia

As partial fulfillment of the requirement to graduate with honors degree in

BACHELOR OF ENGINEERING (MECHANICAL ENGINEERING)

School of Mechanical Engineering

Engineering Campus

Universiti Sains Malaysia

DECLARATION

This work has not previously been accepted in substance for any degree and is not being concurrently submitted in candidature for any degree.

Signed.....

(SITI ROSYADA BINTI MUHAMAD YUSLI)

Date .....

Statement 1

This thesis is the result of my own investigation, except where otherwise stated. Other sources are acknowledged by giving explicit references. Biblography/references are appended.

Signed.....

(SITI ROSYADA BINTI MUHAMAD YUSLI)

Date .....

Statement 2

I hereby give consent for my thesis, if accepted, to be available for photocopying and for interlibrary loan, and for the title and summary to be made available outside organizations.

Signed.....

(SITI ROSYADA BINTI MUHAMAD YUSLI)

Date .....

ACKNOWLEDGEMENT

First and foremost, I would like to thank God Almighty for giving me the strength, knowledge, ability and opportunity to undertake this final year project and to persevere and complete it satisfactorily. Without His blessings, this achievement would not have been possible.

In my journey towards this degree, I have found a teacher, an inspiration, a role model and a pillar of support in my Guide, Dr. Mohd Azmi bin Ismail. He has been there providing his heartfelt support and guidance at all times and has given me invaluable guidance, inspiration and suggestions in my quest for knowledge. Without his able guidance, this thesis would not have been possible and I shall eternally be grateful to him for his assistance.

I would also like to express my gratitude to all lecturers and technical staffs in the School of Mechanical Engineering, Universiti Sains Malaysia, who have been so helpful and cooperative in giving their support at all times and sharing their knowledge to help me achieve my goal.

It would be inappropriate if I omit to mention the names of my dear friends Amirah, Farah, Miza, Aqilah, Intan and Munirah, who have, in their own ways, kept me going on my path to success, assisting me as per their abilities, in whatever manner possible and for ensuring that good times keep flowing.

My acknowledgement would be incomplete without thanking the biggest source of my strength, my family. My parents, Mr. Muhamad Yusli and Mrs. Roziah, who never let things get dull or boring, have all made a tremendous contribution in helping me reach this stage in my life. I thank them for putting up with me in difficult moments where I felt stumped and for goading me on to follow my dream of getting this degree. This would not have been possible without their unwavering and unselfish love and support given to me at all times.

Table of Contents

LIST OF FIGURES

LIST OF TABLES

LIST OF ABBREVIATIONS

SAI	Swirling Anti-Icing
PTAI	Piccolo Tube Anti-Icing
CFD	Computational Fluid Dynamics
FSI	Fluid Structure Interaction
WAI	Wing Anti-Ice
NRA	Nozzle Rotation Angle
$C_{temp\ dev}$	Coefficient of Temperature Deviation
SST	Shear Stress Transport
Re	Reynolds number
ρ	Density
V	Velocity
D_h	Hydraulic Diameter of The Nozzle
μ	Dynamic Viscosity
FEM	Finite Element Modeler

THE NUMERICAL COMPARISON STUDY ON THE EFFECT OF THE ANTI-ICING METHODS ON THERMAL STRESS DISTRIBUTION OF THE NACELLE LIP-SKIN

ABSTRACT

In-flight ice accumulation is a serious hazard. It ruins the smoothness flow of air, increasing drag, degrading control authority and decreasing the ability of an airfoil to lift. The worst situation would be when broken ice particles are absorbed, which ingestion of would break down the engine. This situation shows that anti-icing methods are very important to overcome this problem. Therefore, the main objective of this project is to study the effect of the anti-icing methods on thermal stress distribution of nacelle lip-skin. There are two anti-icing methods that will be compared in this project, which are Swirling Anti-Icing (SAI) and Piccolo Tube Anti-Icing (PTAI) methods. Computational Fluid Dynamics (CFD) has been widely used to study the effect of ice accretion onto the nacelle lip skin. CFD analysis can help to save time and effort, as well lower the cost by reducing the number of experiments required during the development. In order to achieve the main objective, the fluid structure interaction (FSI) is utilized. ANSYS Fluid Flow (FLUENT) is used in this project to study the thermal distribution and it will be paired with static structural to investigate any mechanical deformation. Simulation results shows that the SAI is a better anti-icing system compared to PTAI as the maximum stress value is lower than PTAI. Aluminium 2 series is chosen as the best material because it has the lowest value of the maximum strain.

KAJIAN PERBANDINGAN NUMERIKAL KE ATAS KESAN KAEDAH-KAEDAH ANTI-PENGAISAN TERHADAP PENGAGIHAN TERMA STRESS DI BIBIR NACELLE

ABSTRAK

Pengumpulan ais semasa penerbangan adalah bahaya yang sangat serius. Hal ini menganggu kelancaran aliran udara, meningkatkan daya seret, merendahkan kawalan kuasa dan menurunkan keupayaan sesuatu airfoil untuk mengangkat. Situasi yang paling teruk adalah apabila zarah ais yang pecah, dimamah lalu merosakkan enjin. Situasi ini menunjukkan bahawa kaedah-kaedah anti-pengaisan ini sangat penting untuk mengatasi masalah ini. Oleh itu, objektif utama projek ini adalah untuk mengkaji kesan kaedah-kaedah anti-pengaisan terhadap pengagihan terma stress di bibir nacelle. Terdapat dua kaedah anti-pengaisan yang akan dibandingkan dalam projek ini, iaitu kaedah anti-pengaisan pusaran dan kaedah anti-pengaisan tiub piccolo. Pengkomputaran Dinamik Bendalir telah digunakan secara meluas untuk mengkaji kesan pertambahan ais pada bibir nacelle. Analisis CFD dapat membantu menjimatkan masa dan usaha, serta mengurangkan kos dengan mengurangkan bilangan eksperimen yang diperlukan semasa pembangunan. Untuk mencapai objektif utama, interaksi struktur bendalir (FSI) digunakan. ANSYS Aliran Bendalir (FLUENT) akan digunakan dalam projek ini untuk mengkaji pengagihan terma dan ianya akan dipadankan dengan struktur static untuk menyiasat sebarang perubahan bentuk mekanikal. Hasil simulasi menunjukkan bahawa kaedah anti-pengaisan pusaran ialah kaedah anti-pengaisan yang lebih baik berbanding dengan kaedah anti-pengaisan tiub piccolo kerana nilai stress maksima lebih rendah daripada kaedah anti-pengaisan tiub piccolo. Alumina 2 series telah dipilih sebagai bahan yang terbaik kerana ia mempunyai nilai maksima ketegangan yang paling rendah.

CHAPTER 1

INTRODUCTION

1.1 PROJECT OVERVIEW

In-flight ice accumulation is a serious hazard. It ruins the smoothness flow of air over the wing and tail, increasing drag, degrading control authority and decreasing the ability of an airfoil to lift. Ice typically builds up when tiny cloud droplets impact and freeze on the leading edges, or front surfaces, of the plane. The actual weight of the ice on the aeroplane is secondary to the airflow disruption it causes. As power is added to compensate for the additional drag and the nose is lifted to maintain altitude, the angle of attack increases, allowing the underside of the wings and fuselage to accumulate additional ice [1]. In moderate to severe conditions, a light aircraft can become so iced up which is impossible to continue its flight.

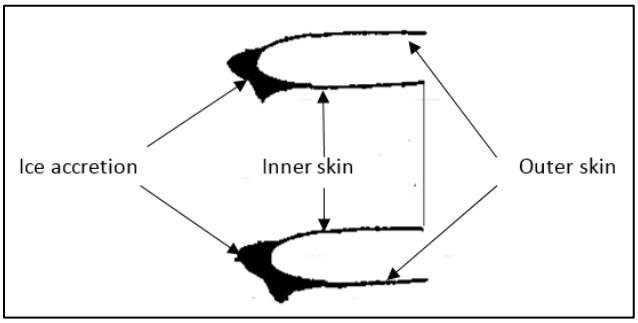

Figure 1.1: Ice accretion on the underside of nacelle lip-skin [2]

There are various systems in use to prevent the formation of ice, and these are mostly based on mechanical, chemical or thermal techniques. Some of these systems are anti-icing and de-icing mechanisms. . Anti-icing is pre-emptive mechanism. It is turned on before the flight enters the icing conditions. Examples of anti-icing system are thermal heat, prop heat, pitot heat, fuel vent heat, windshield heat, and fluid surface de-icers. Meanwhile, de-icing is reactive mechanism. It is used after there has been significant ice build-up Examples of surface de-ice equipment such as boots, weeping wing systems, and heated wings. [3]

The thermal bleed technique is the most popular technique in aircraft industry. For PTAI system, a piccolo tube, with a series of in-line or staggered holes, is placed inside the wing leading end near to its inner surface. The hot air, bled out from the engine compressor, is passed through the piccolo tube, and it ejects from the piccolo tube holes in the form of high velocity jets that impinge on to the inner surface of the wing leading edge. Subsequent heat conduction from wing inner surface to outer surface results in maintaining the outer surface of the wing leading edge hot enough to avoid accretion of ice. [4]

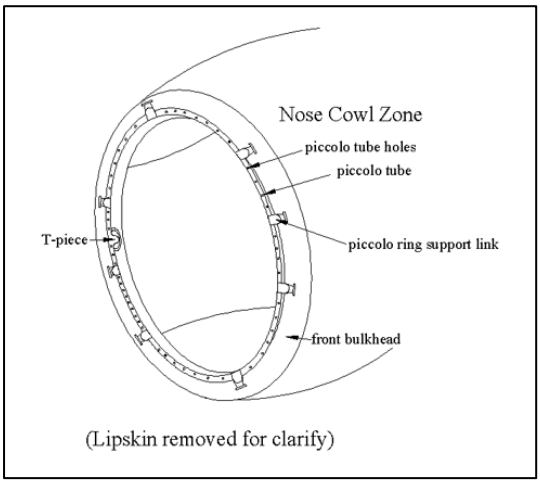

Figure 1.2: Piccolo tube anti-icing system [5]

Furthermore, in SAI system, a nozzle is placed at the certain plane angle in the nacelle lip-skin. Similar to the PTAI system, the hot air is bled out from the engine compressor and it ejects from the nozzle in the form of high velocity jets that impinge on to the inner surface of the nacelle lip-skin. The hot air will swirl in the nacelle lip-skin and transfer heat energy to the cold air to avoid accretion of ice at the lip-skin.

The anti-icing systems may help the aircraft to avoid an accident due to ice accumulation. However, there are some issues with these systems. The hot air that impinges on the nacelle lip-skin may influence the thermal and mechanical properties of the nacelle lip-skin. Rapid heat transfer from the nozzles onto the nacelle lip-skin will cause the temperature of the lip-skin to increase rapidly. Therefore, it possesses an effect to the material of the nacelle lip-skin which will change the mechanical properties of the lip-skin.

The variation in mechanical properties can pose a direct threat to nacelle lip-skin as when it deforms, it will alter the original shape of the lip-skin resulting a significant change in aerodynamic properties of the geometry. Hence it is vital to study the effect of hot gas flow from Piccolo Tube Anti-Icing (PTAI) and Swirling Anti-Icing (SAI) in term of material deformation and thermal stress on the nacelle lip-skin, so that we can predict the nacelle lip-skin life expectancy.

1.2 PROBLEM STATEMENT

The anti-icing methods by impinged the hot gas into the nacelle lip-skin seem to be the most popular technique to solve in-flight ice accumulation. This is because there are a few advantages of this method such as increased safety, reduced deicer use and labor and cost savings [6]. However, we cannot neglect the disadvantage of these methods which can lead to the serious problem. The hot air that impinges on the nacelle lip-skin may influence the thermal and mechanical properties of the nacelle lip-skin. As there are sudden increase in the lip-skin temperature, the material of the nacelle lip-skin may be affected when the heat is transferred rapidly from the nozzle to the lip-skin. This situation is possible to assist the changes of mechanical properties of the lip-skin. Therefore, the main objective is to study the numerical comparison on the effect of the anti-icing methods, which are Swirling Anti-Icing (SAI) and Piccolo Tube Anti-Icing (PTAI), on thermal stress distribution of the nacelle lip-skin.

1.3 OBJECTIVES

The objectives of this project are stated below:

- To quantify the effect of the anti-icing methods on thermal stress distribution of nacelle lip-skin
- To determine the thermal characteristics of aluminium (1 series, 2 series and 7 series)
- To identify the most suitable material of the nacelle lip-skin

1.4 SCOPE OF THE PROJECT

The anti-icing system usually install at many parts of the aircraft. However, this project only focus on the anti-icing systems, which are Piccolo Tube Anti-Icing (PTAI) system and Swirling Anti-Icing (SAI) system, at the nacelle lip-skin part. Others are neglected. Computational Fluid Dynamic (CFD) will be a main tool to be used in studying the deformation and properties change of the lip-skin. Therefore, the fluid-structure interaction (FSI) method is utilized to investigate the effect of the swirling anti-icing and the piccolo tube anti-icing on thermal stress distribution of the nacelle lip-skin. The most suitable type of aluminium for material of the lip-skin will be determined after analyse the results obtained.

CHAPTER 2

LITERATURE REVIEW

2.1 INTRODUCTION

The literature review basically reviews the previous studies on related topics to this project. The topics that are related include ice formation on aircraft, aircraft crash, fundamental of anti-icing system and application of CFD in this study.

2.2 ICE FORMATION ON AIR CRAFT

In aviation, the icing conditions are those atmospheric conditions which may lead to the accumulation of water ice on the surface of the aircraft. The most often causes that lead to ice formation on the external components of an aircraft is the effect of the impact of supercooled water droplets of various sizes on that air craft. This can be happen when the air craft is in the cloud or flying through precipitation. The water droplets do not all freeze when the ambient temperature falls below 0°C and often exists as a "supercooled" liquid. This is because the release of latent heat during the change of water state to ice.

In-flight icing condition is very dangerous as it can lead into a serious accident. Ice builds up destroys the smooth flow of air, increasing drag, degrading control authority and decreasing the ability of an airfoil to lift. The additional weight and unequal formation of the ice can cause unbalancing of the aircraft, which making it hard to control. Table 2.1 shows the summary of the air crash occur due to ice. From year 2000 to 2018, there are at least 17 air crash due to ice. The worst scenario is that ice on the wing breaks off during takeoff due to the flexing of the wing and goes directly into the engine, leading to surge, vibration, and complete thrust loss. Light snow that is loose on the wing surfaces and the fuselage can also cause engine damage leading to surge, vibration, and thrust loss.

Table 2.1: The summary of the air crash occur due to ice [7]

Year	Site	Air Carrier	Aircraft	Phase
1982	U.S.A	Air Florida	Boeing 737-222	Takeoff
1985	Canada	Arrow Air	McDonnell-Douglas DC-8-63CF	Takeoff
1985	Russia	Aeroflot	Tupolev TU-134A	Landing
1987	U.S.A	Continental Airlines	McDonnell-Douglas DC-9-14	Takeoff
1989	Canada	Air Ontario	Fokker F-28	Takeoff
1991	U.S.A	Ryan Airlines	McDonnell-Douglas DC-9-15RC	Takeoff
1991	Russia	Aeroflot	Antonov AN-12B	Landing
1991	Russia	Tartarstan Airlines	Antonov AN-24	Landing
1992	U.S.A	USAir	Fokker F-28	Takeoff
1993	Macedonia	Palair Macedonian	Fokker 100	Takeoff
1994	U.S.A	American Eagle	ATR 72-212	Landing
1994	Russia	North Western Air Transport	Antonov AN-12B	Landing
1995	Italy	Romanian Banat Air	Antonov AN-24B	Takeoff
1997	U.S.A	Comair Airlines	Embraer EMB120-Brasilia	Landing
1998	Canada	Private	CRJ-200LR	Takeoff
1999	Turkey	Turkish Airline	Boeing 737-400	Takeoff
2000	Russia	Vologodskiye Airline	Yakovlev YAK-40	Takeoff
2002	U.K.	Private	Bombardier CL-600-2B16	Takeoff
2004	U.S.A	Private	Bombardier CL-600-2A12	Takeoff
2004	China	China Eastern Airlines	Bombardier CRJ-200LR	Takeoff
2005	U.S.A	Private	Cessna Citation 560	Landing
2006	China	China PLA Air Force	KJ-200	Landing
2007	Russia	Private	Bombardier CL-600-2B16	Takeoff
2008	Armenia	Belavia	Bombardier CL-600-2B19	Takeoff
2008	U.K	British Airways	Boeing 777-236ER	Landing
2009	U.S.A	Colgan Air	Bombardier DHC8-402 Q400	Landing
2009	Altantic Ocean	Air France	Airbus A330-203	Takeoff
2012	Siberia	UTAir	ATR 72-201	Takeoff
2014	Mali	Air Algérie	McDonnell Douglas MD-83	Takeoff

2014	Maryland	Private	Embraer EMB-500 Phenom	Landing
2015	Canada	Wasaya Airways	Cessna 208B Grand Caravan	Takeoff
2017	Myanmar	Myanmar Air Force	Shaanxi Y-8F-200	Landing
2018	Moscow	Saratov Airlines	Antonov An-148-100B	Landing

There are several types of ice that accumulate on the air craft such as rime, clear or glaze and mixed. Rime ice has a rough milky appearance and generally follows the surface closely. Clear or glaze ice is sometimes clear and smooth but usually contain some air pockets that result in a lumpy translucent appearance, denser harder and more difficult to break than rime ice.

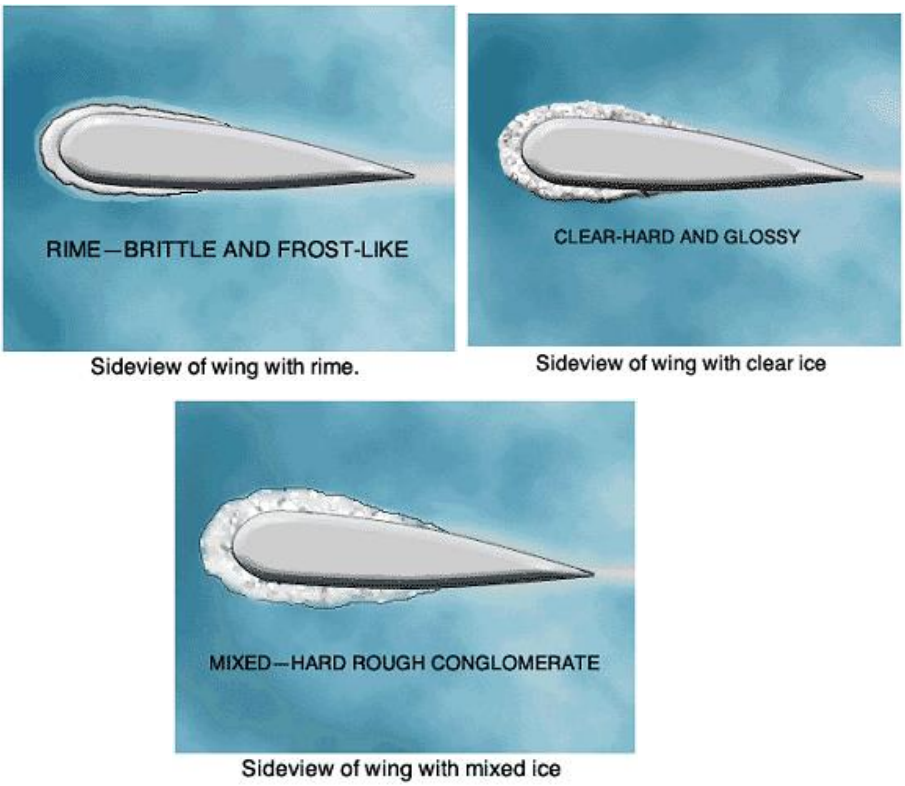

Figure 2.1: Three different types of ice

2.3 ICE PREVENTION

Formation of ice can be detected visually. However, the most modern aircraft have one or more ice detector sensors that warn the flight crew of icing conditions. An annuciator light comes on to alert the flight crew. There are two types of ice removal

such as anti-icing and de-icing. Several equipment is designed for anti-icing and deicing system. This is to prevent or control the ice formation on the aircraft. Anti-icing equipment is turned on before the flight entering the icing conditions and it is designed to prevent ice form forming. A surface may be anti-iced by keeping it dry, by heating to a temperature that evaporate water upon impingement or by heating the surface just enough to prevent the ice formation. Examples of anti-icing are thermal heat anti-icing, wing anti-ice (WAI) system, thermal electric anti-icing, chemical anti-icing, piccolo tube anti-icing and swirl anti-icing.

For thermal heat anti-icing mechanism, air heated is bled air from engine heats inlet cowls to keep ice from forming. Bleed air can be ducted to wings to heat wing surface as well.

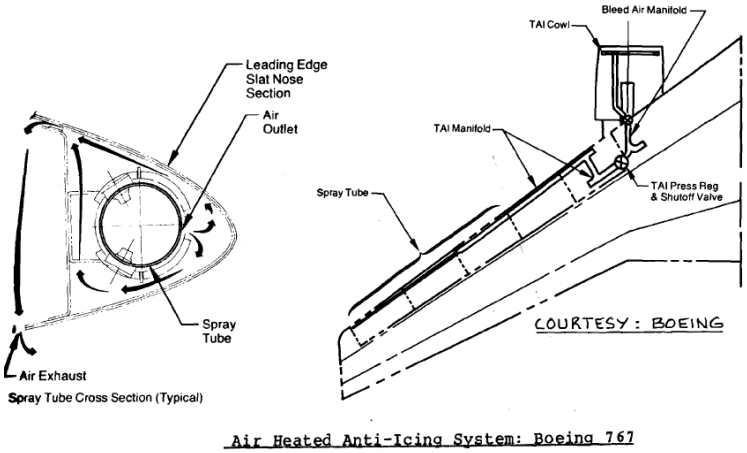

Figure 2.2: Air heated anti-icing system
(Airplane Design, Book 4, Roskam)

De-icing equipment is designed to remove ice after it begins to accumulate on the wings and stabilizer leading edges. The examples of surface de-ice equipment are boots, weeping wing systems and heated wings.

For boots de-icing mechanism, there are inflatable rubber strips that run along the leading edge of wing and tail surfaces. When inflated, they expand knocking ice off of wing surface. After ice has been removed, suction is applied to boots, returning them

to the original shape for normal flight. This type of de-icing mechanism is usually used on smaller planes. [3]

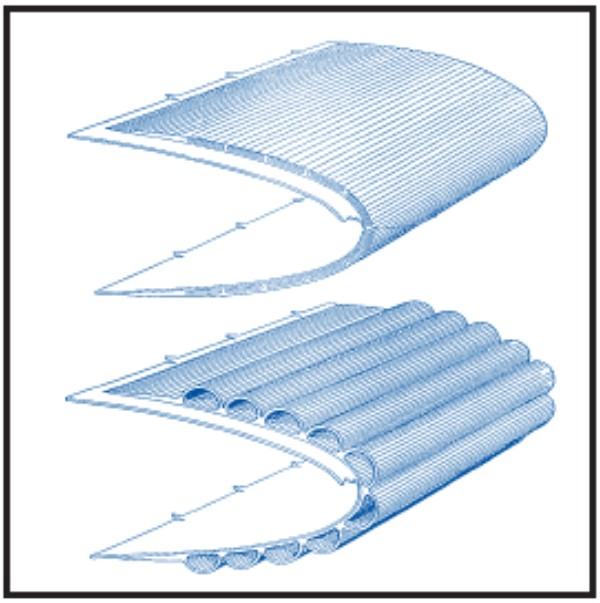

Figure 2.3: Boots de-icing system [3]

Hot bleed air anti-icing systems, particularly SAI and Piccolo Tube Anti-Icing (PTAI), have been used as nacelle ice protection mechanism in commercial aviation. [8] PTAI is one of the most popular hot bleed air anti-icing devices utilized in wing and nacelle anti-icing systems. It is the most efficient and reliable anti-icing system. There are several holes along the piccolo tube that will impinge the hot gas onto the nacelle lip-skin. The hot air mass flow rate, jet spacing, the distance from the holes to the surface and the impingement angle are the parameters affecting the thermal performance of the PTAI. This high performance preventive system is better than other ice protection systems with respect to the efficiency, but has limitations in terms of performance losses, energy cost, complexity, weight and hotspot issues.

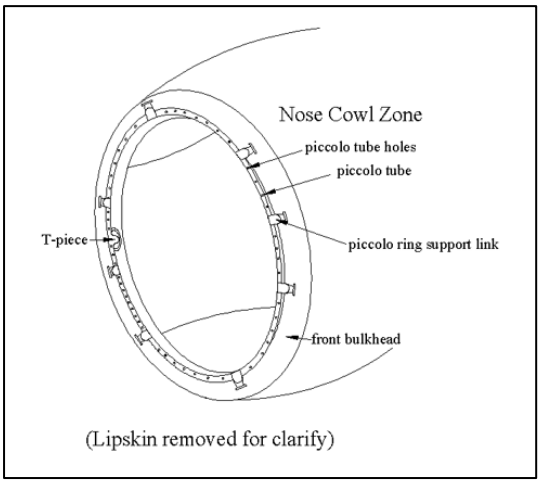

Figure 2.4: Piccolo tube anti-icing system [5]

The second type of anti-icing system is Swirl Anti-Icing (SAI). The SAI is an alternative hot air anti-icing mechanism, has the potential to overcome hotspot problems. The SAI is an effective anti-icing mechanism (Herman, 1987), capable of providing uniform temperature distributions along the nacelle lip. As a result, less runback ice develops on the downstream area (Rosenthal and Nevepovitz, 1985). [9] There is a nozzle in the D-chamber of the nacelle lip-skin that will impinge the hot gas onto the lip-skin. The hot gas is bled from the engine and the compressor, and will flow into the nozzle via the inlet nozzle. After the hot gas flow out from the nozzle and collide with the inner wall of the lip-skin, the hot gas then swirl in the lip-skin.

2.4 EFFECT OF NOZZLE ROTATION ANGLE TO COEFFICIENT OF TEMPERATURE DEVIATION

According to the previous study, in Swirling Anti-Icing (SAI) systems, nozzle rotation angle (NRA) is one of the factors that affect the coefficient of temperature deviation of the nacelle lip-skin. This study is done by rotating the nozzle toward the inner skin of the lip-skin by giving several degrees of angle. When the nozzle direction is more towards the inner skin, the distance between nozzle outlet and the impinging point decreases. As a result, the hotspot temperature decreases. This is because the mixing process is enhanced due to the increase in momentum and heat exchange between hot air and cold air in the D-chamber.

There are five different angles used in this study such as 0°, 5°, 7°, 9° and 13°. Based on this study, the temperature of the hotspot decreases and the cold spot increases as the NRA increases. Therefore, the 13° rotation shows the best temperature uniformity of the SAI system since it has the lowest $C_{temp\ dev}$ in this study. [8]

2.5 EFFECT OF NOZZLE LENGTH ON COEFFICIENT TEMPERATURE DEVIATION

Based on previous study, nozzle length in SAI system can affect the coefficient temperature deviation. The researcher used five different nozzle length (1 diameter (1d), 1.5-diameter (1.5d), 2-diameter (2d), 2.5-diameter (2.5d) and the original length (3d) for a single nozzle with a diameter of 9.144×10^{-3}m) to investigate the temperature distribution of the nacelle lip-skin. When the nozzle length change, the distance between the nozzle outlet and the hotspots change. Since the hot gas from the nozzle requires some space to mix well with the stagnation air in the D-chamber, the nozzle length plays important role in this SAI system. Results show that the shorter nozzle length improves a nacelle lip-skin's temperature distribution uniformity. However, this improvement is not significant as 1.5d nozzle produces the smallest cold spot area. [8]

2.6 COMPUTATIONAL FLUID DYNAMIC

Computational Fluid Dynamic (CFD) is a reliable tool, used to predict an assortment of issues, including heat transfer, fluid flow, and combustion. Currently, a larger number of researchers are using CFD codes as a first step in designing or studying anti-icing systems. By using CFD, researchers can reduce the number of tests, as well as the cost associated with physical experiments and, at the same time, study some parameters that cannot obtained from the experiment. [10]

CHAPTER 3

METHODOLOGY

3.1 INTRODUCTION

This chapter will describe the simulation process of nacelle lip-skin assisted by ANSYS Workbench 14.0. Fluid-structure interaction (FSI) method is used to study the thermal stress distribution of nacelle lip-skin. By using ANSYS Fluid Flow (FLUENT), the maximum temperature of nacelle lip-skin is monitored.

3.2 GEOMETRY

In this project, the nacelle lip-skin model is based on the Falcon 20g Nacelle Lip-skin. The geometry of the nacelle lip-skin is obtained from the previous researcher. The schematic of the Falcon 20g nacelle D-Chamber are shown in Figure 3.1 and 3.2 respectively.

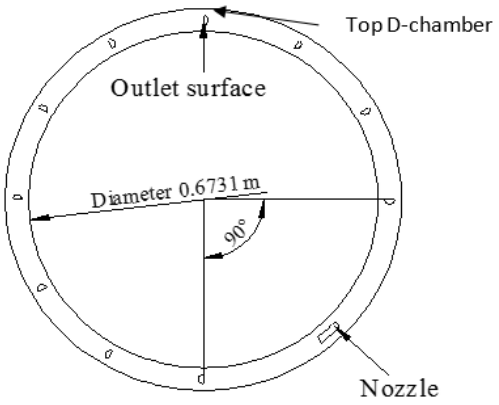

Figure 3.1: Schematic drawing of Falcon 20g nacelle D-Chamber

The design of SAI system consists of 10 exhausts, which are in a semicircular shape and had a diameter of 0.0381m. Based on Figure 3.1, 10 exhausts are located on the bulkhead, 30° apart from each other and ±45° apart from nozzle inlet point. The nacelle inlet diameter is 0.672m, while the nozzle diameter and length are 0.0170688m

and 0.027432m respectively. The nozzle and bulkhead are built with stainless steel and titanium.

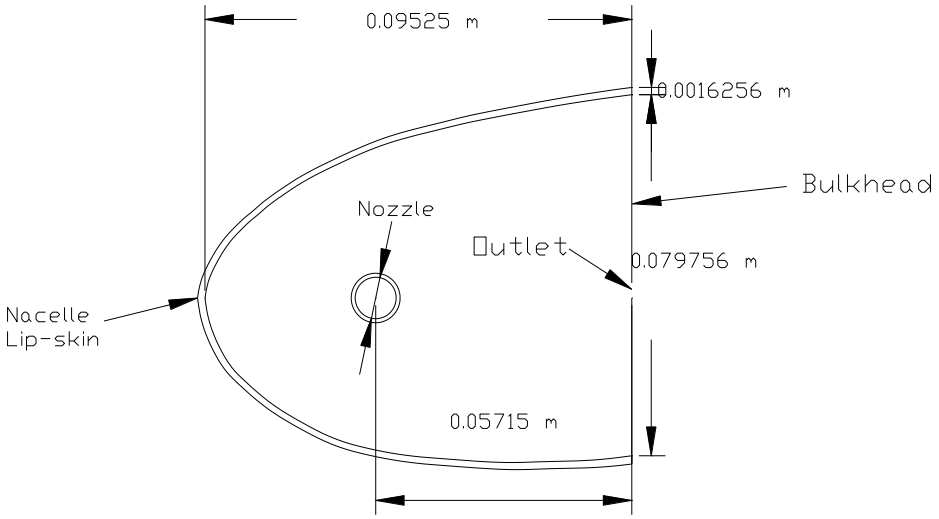

Figure 3.2: Schematic drawing of a cross section of nacelle lip-skin

Figure 3.2 shows the nacelle lip-skin cross-section in plane 140°. The height of the bulkhead and the length of the D-chamber were 0.079756m and 0.09525m respectively. The nozzle was placed 0.05715m in front of the bulkhead and nacelle lip-skin thickness is of 0.0016256m.

The geometry and meshing are done assisted by GAMBIT pre-processor before importing into ANSYS Workbench. Figure 3.4 illustrates the positions of planes, in degrees, in the nacelle D-chamber.

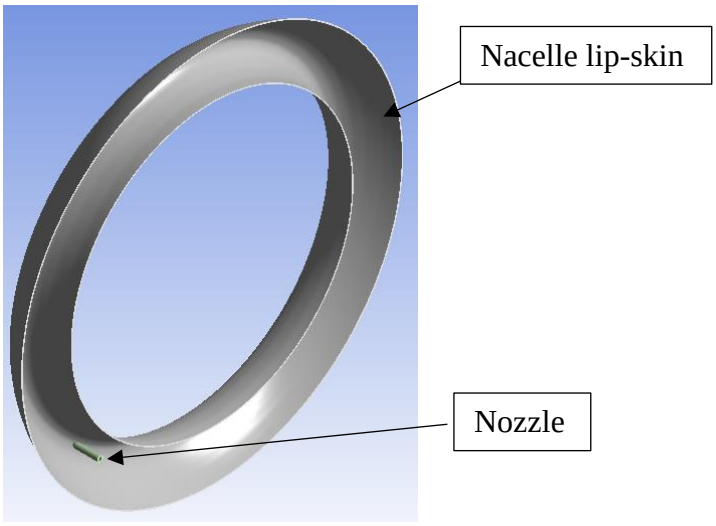

Figure 3.3: Overall geometry of nacelle lip-skin

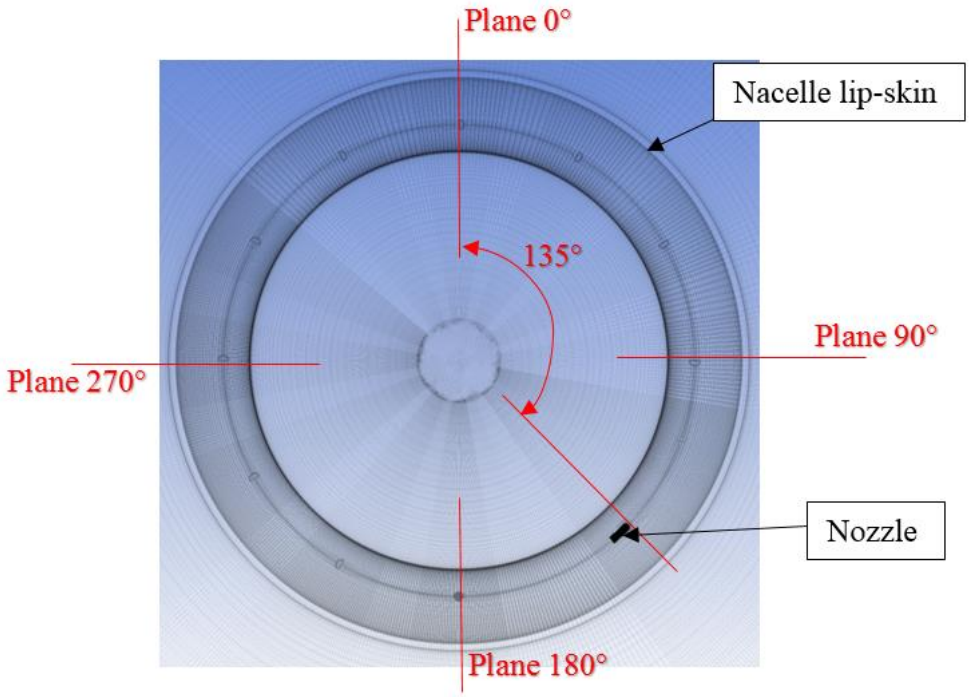

Figure 3.4: Plane position on the nacelle lip-skin

3.3 MESHING AND BOUNDARY CONDITION

The meshing of SAI nacelle lip-skin is created in the GAMBIT pre-processor, which included naming the surface and boundary conditions for the faces. More than 4.6×10^6 linear hexahedron elements are used during this simulation process.

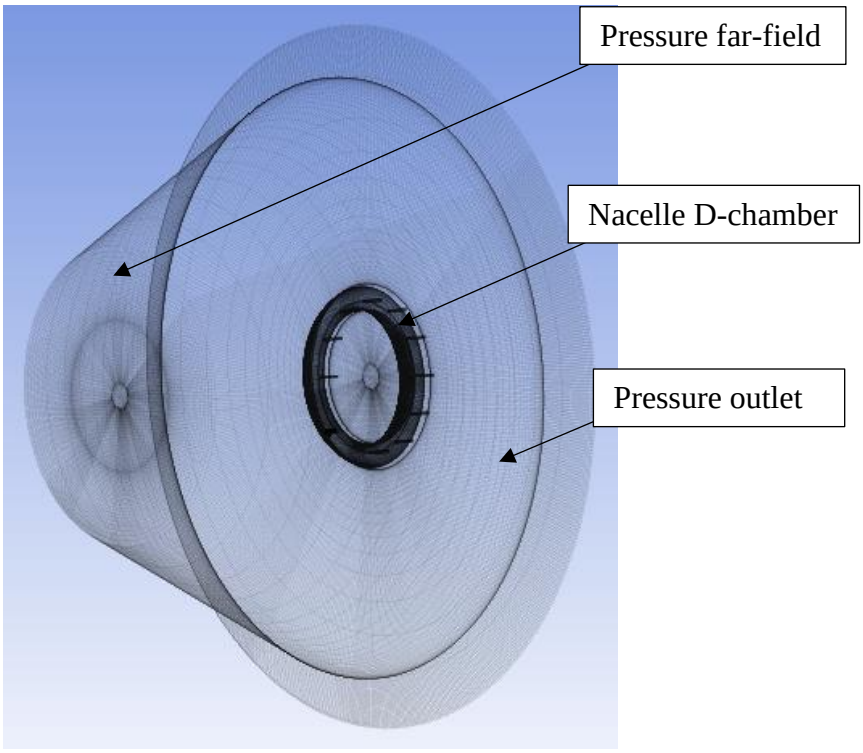

Figure 3.5: Boundary condition of swirl anti-icing

A pressure outlet is used on the rear surface ambient domain in order to release the free stream flow inside the ambient domain. Pressure far field is utilized as the controller of the free stream velocity. Based on figure 3.6, there are ten pressure outlets inside the nacelle lip, which used to release the exhausted hot air from the D-chamber to the ambient. These outlet surfaces are extended to prevent the backflow phenomenon inside the D-chamber. The mass-flow-rate boundary condition is utilized on the nozzle (small yellow disc in Figure 3.6) inlet in order to control the total temperature and the mass-flow-rate of the hot air entering the SAI system. [3]

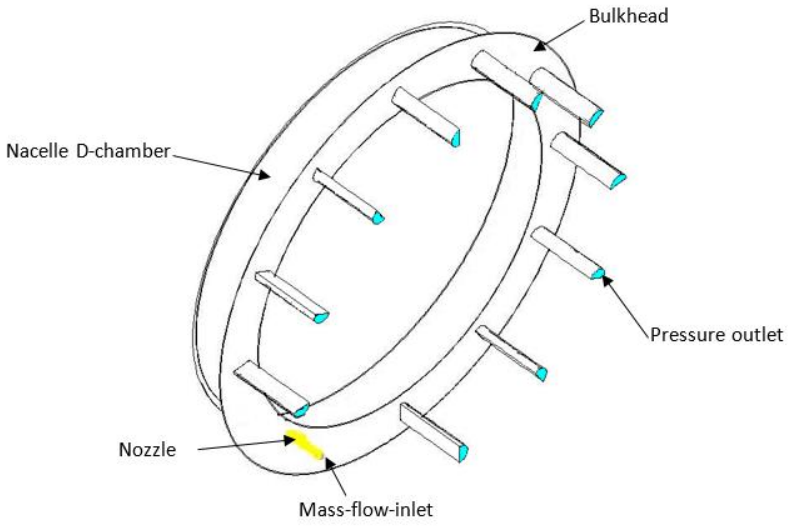

Figure 3.6: Boundary condition inside D-chamber [3]

3.4 ANSYS FLUENT SIMULATION

The geometry of the nacelle lip-skin drawn in Gambit pre-processor is imported into Ansys FLUENT for CFD simulation. The SST K-omega (k-ω) turbulence model is chosen as it is well suited for simulating flow in the viscous sub-layer. The SST k-ω model has a better performance in transitional flows and in flows with adverse pressure gradients. The SST model incorporates a damped cross diffusion derivative term in the ω equation. Hence, SST k-ω are able to provide a better accuracy of simulation result.

Ten different values of mass flow rate are used in this simulation to study the effect of the anti-icing methods on thermal stress distribution of the nacelle lip-skin. There are 0.1kg/s, 0.2kg/s, 0.31255kg/s, 0.46611kg/s, 0.6196kg/s, 0.773239kg/s, 0.931224kg/s, 1.080366kg/s, 1.23393kg/s and 1.38749kg/s. For the first simulation, mass flow rate of 0.1000kg/s is inserted. For the pressure far field, turbulence intensity (constant) was specified at 2% and the operating conditions are at 68051 Pa. For hot gas inlet boundary, the turbulent intensity was set at 7% intensity and operates at same operating conditions as pressure far field. The temperature of the hot gas is 545.15K. Table 3.1 shows the summary of the boundary condition used in this project.

Table 3.1: Summary of boundary condition

CFD Software	FLUENT 6.3.26
Turbulent flow model	*SST* k-ω
Type of flow	Ideal gas (compressible)
Energy Equation	On
Velocities of free stream air	0.149
Temperature of Free Stream Air	276.16K
Mass Flow hot air	0.1000 kg/s
Temperature of hot air	545.15K
Operating pressure	68051 Pa

The calculation is initiated with 2500 iterations using second order upwind. The second order upwind method produce more accurate results compared to first order upwind. The solution is fully converged after 2500 iterations.

After calculation is completed, the next steps are done in the CFD-Post. Temperature contour of the nacelle lip-skin (figure 3.7) is created in order to monitor the location of the hotspot and the temperature of the hotspot. The temperature of the nacelle lip-skin is then recorded and tabulated. Some parameters such as density, velocity and dynamic viscosity of the hot gas are obtained from this simulations.

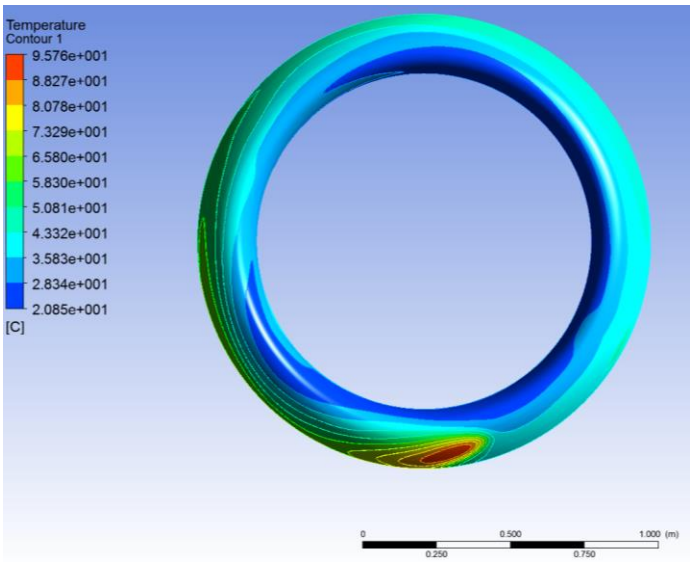

Figure 3.7: Temperature contour of the nacelle lip-skin.

In CFD-Post, one plane is created to identify the velocity contour of the nacelle lip-skin, Figure 3.8. This process is done to ensure that the hot gas nozzle is done the right things.

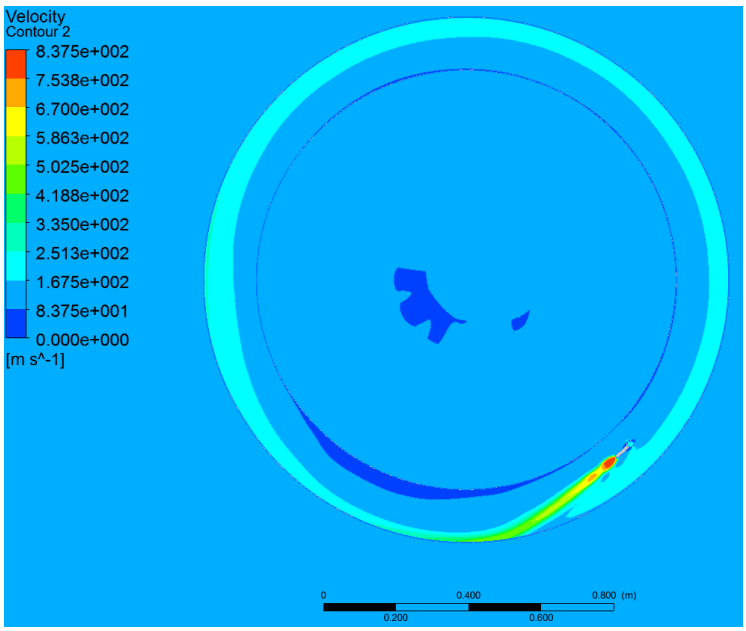

Figure 3.8: Velocity contour of the nacelle lip-skin

The Reynolds number of the hot gas is calculate based on the equation below:

$$Re = \frac{\rho V D_h}{\mu} \quad (1)$$

ρ = density of the hot gas

$V = velocity\ of\ the\ hot\ gas$

$D_h = hydraulic\ diameter\ of\ the\ nozzle$

μ = dynamic viscosity

3.5 FINITE ELEMENT MODELER AND STATIC STRUCTURAL

Finite Element Modeler (FEM) is utilized to import the geometry and meshing of the design model into the Ansys Mechanical. FE Modeler is a module developed to

handle some of the mesh based capabilities found in Mechanical APDL that do not really fit into the ANSYS Mechanical. Figure 3.9 shows the geometry and meshing of the model. Note that the imported mesh is the same as the mesh found in FLUENT simulation.

In the static structural, the imported geometry does not involve any fluid domain and depend on the solid domain only. However, as the FSI method is utilized in this project, the results in static structural is affected by any results from the CFD simulation.

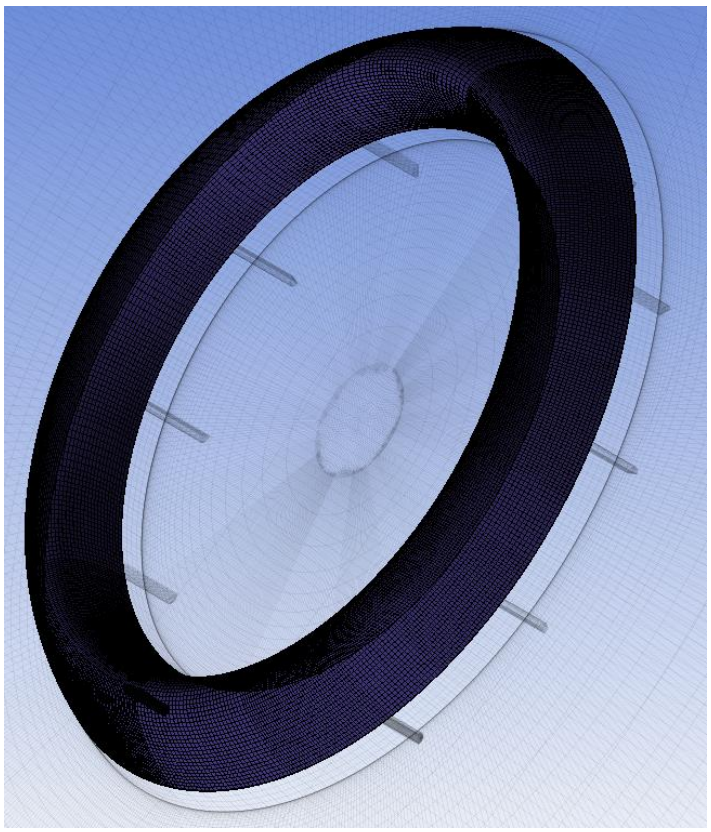

Figure 3.9: Nacelle lip-skin meshing in FEM

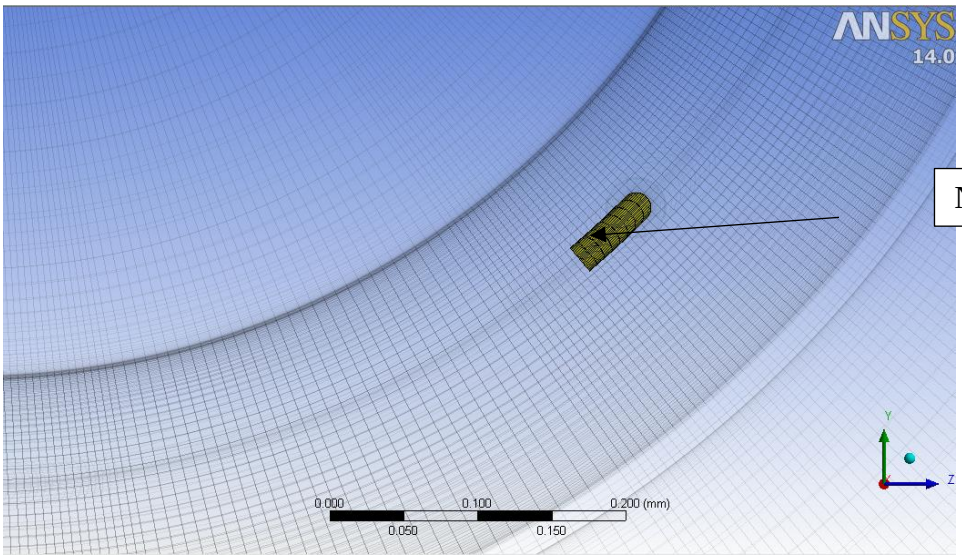

Figure 3.10: Nacelle lip-skin meshing in FEM

Three different series of aluminium is used to study the thermal distribution of the nacelle lip-skin. There are Aluminium 7075-T6 series, 2024-T4 series and 1100-O series. The material properties used in this study are inserted into the engineering data cell. Table 3.2 shows the properties of the aluminium 3 series.

Table 3.2: The properties of the aluminium 3 series.

Properties	**AL 1100-O**	**AL 2024-T4**	**AL 7075-T6**
Density (kg/m^3)	2707	2785	2804
Coefficient of thermal expansion (1/°C)	2.36×10^{-5}	2.28×10^{-5}	2.32×10^{-5}
Reference Temperature (°C)	20	20	20
Young's Modulus (Pa)	6.89×10^{10}	7.31×10^{10}	7.17×10^{10}
Poisson's Ratio	0.33	0.33	0.33
Tensile Yield Strength (MPa)	110	324	503
Tensile Ultimate Strength(MPa)	124	469	572

In the static structural, only the nacelle lip-skin is studied (figure 3.11). Therefore, other parts such as nozzle, bulkhead and exhausts are suppressed. Then, the material is set into the lip-skin. Both pressure and body temperature are imported into the model. Equivalent elastic strain (von Mises) and equivalent stress are generated.

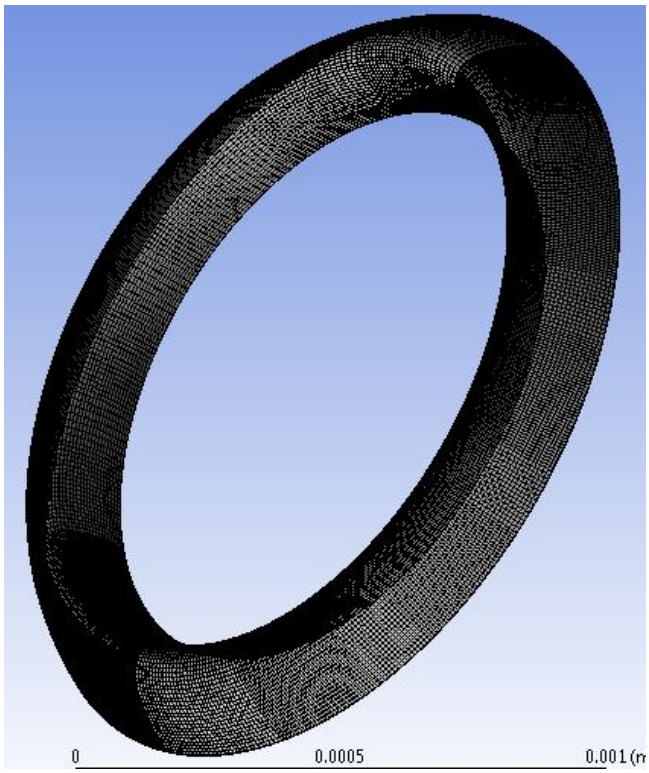

Figure 3.11: Nacelle lip-skin in static structural

The thermal distribution of the nacelle lip-skin is studied based on the results of stress and strain generated in this Ansys Mechanical. Figure 3.12 and 3.13 shows the stress and strain distribution on the nacelle lip-skin.

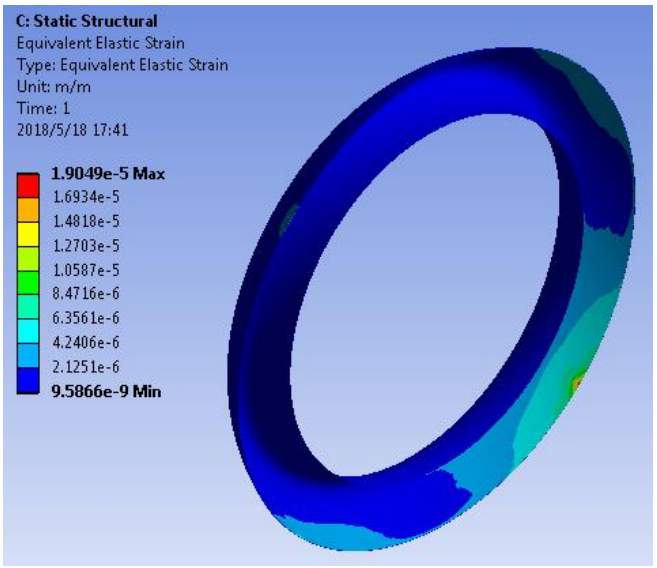

Figure 3.12: Strain distribution of the nacelle lip-skin

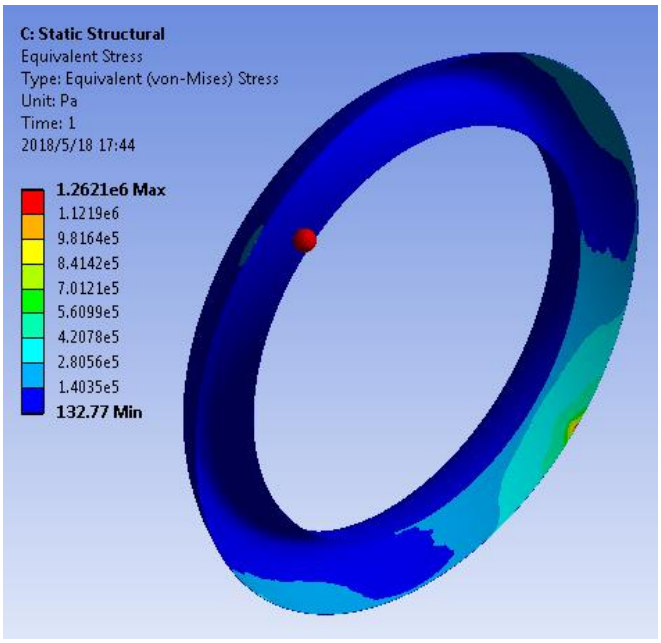

Figure 3.13: Stress distribution of the nacelle lip-skin

The maximum stress and strain for ten mass flow rate are then recorded and tabulated.

CHAPTER 4

RESULTS AND DISCUSSION

4.1 INTRODUCTION

This chapter discusses the results and discussions of SAI simulations done in ANSYS FSI. The simulation results obtained are compared with the results of previous study, which is PTAI system. The relationship between anti-icing methods and thermal stress distribution of the nacelle lip-skin are discussed. The thermal characteristics of aluminium (1 series, 2 series and 7 series) are determined.

4.2 ANSYS FLUENT SIMULATION ANALYSIS

The simulation is done to identify the thermal stress distribution of the nacelle lip-skin assisted by ANSYS FSI. In this study, the nozzle length, nozzle diameter, nozzle rotational angle and temperature of hot gas are constant. The first parameter that being study in this project is temperature distribution of the lip-skin. Figure 4.1 shows the temperature distribution of the nacelle lip-skin obtained for ten different mass flow rate. According to figure 4.1, there is a hotspot occurs at point A. Hotspot occurs due to the hot air exiting from the nozzle and directly impinging on point A. As a result, the thermal and hydraulic boundary layer becomes very thin causing the highest heat transfer occurs at this spot. After the hot gas impinges the outer skin of the lip-skin, it changed its direction and flow along the nacelle D-chamber. Simulation results show that when the mass flow rate of the hot air increases, the temperature along the outer skin increases. This statement can be proven when the temperature at point B increases.

The momentum of the hot gas become highest when the mass flow rate of the hot gas increases. This causes the hot gas to impinge the outer skin of the nacelle, thus, transfer the heat and kinetic energy there as much as possible. As a results, the outer

skin of the lip-skin has the highest temperature compared to the inner skin. The hotspot temperature readings are then recorded and plotted as shown in figure 4.2. The graph shows that when the mass flow rate of hot gas increases, the hot spot temperature increases. The cold spot temperature readings also recorded and tabulated (figure 4.3). The line graph shows that the cold spot temperature increases until mass flow rate of 0.931224 kg/s before decreasing at mass flow rate of 1.080366 kg/s. However, after mass flow rate of 1.080366 kg/s, the cold spot temperature increases. This phenomenon shows that when the mass flow rate of hot air increases, the hot air has better opportunity to mix with the cold air in the D-chamber as it transfers more heat and momentum to the cold air.

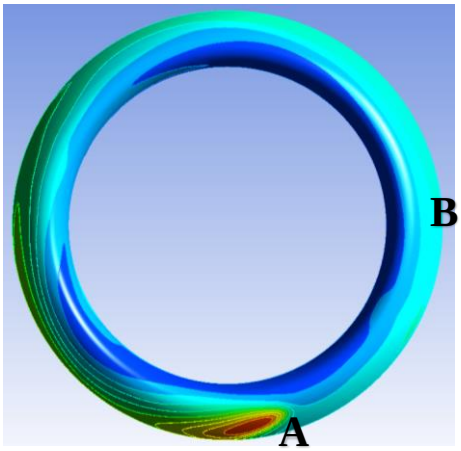

(a) 0.1 kg/s

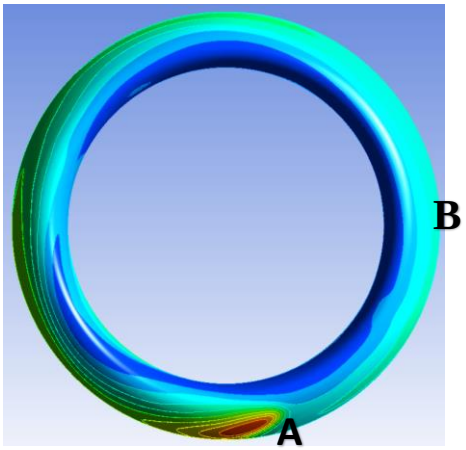

(b) 0.2 kg/s

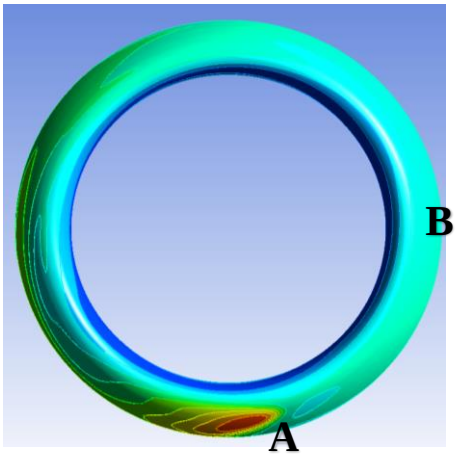

(c) 0.31225 kg/s

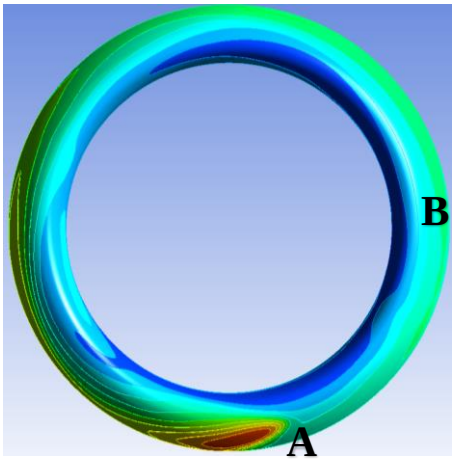

(d) 0.46611 kg/s